Carbonates and Evaporites (2024) 39:82
https://doi.org/10.1007/s13146-024-00994-x

ORIGINAL ARTICLE

# Trace element geochemistry of magnetite from the Mahura iron placer deposit, Markazi province, Iran: implications for magnetite provenance rocks

**Elham Firouzi[1] · Farhad Ehya[2] · Mohammad Ali Aliabadi[1] · Razieh Mohammadi[3]**

Accepted: 8 July 2024


## Abstract

The Mahura iron placer deposit is located 55 km northeast of Arak city in the Markazi province, Iran. From a geological point of view, it is located in the Central Iran Zone. In this study, the trace element geochemistry of magnetite is used to determine the origin of placer magnetites in the Mahura deposit. Magnetite is the most important placer mineral that occurs as micrometer-sized grains in the Quaternary alluvium. The alluvium consists of sandy, silty and clayey sediments containing a considerable amount of volcanic rock fragments of various sizes. The results of the petrographic studies and the whole-rock geochemistry indicate that the volcanic rock fragments are mostly andesite and basaltic andesite. These volcanics contain 4 to 10% magnetite as disseminated grains in the groundmass and as inclusions in plagioclase and amphibole phenocrysts. The mineral chemistry of the placer magnetites indicates 2.59–3.33% Ti, so that they can be considered as titanomagnetite or as a solid solution between magnetite and ilmenite. The chemical composition of the magnetites in the volcanic rock fragments also falls within the range of titanomagnetite with a tendency towards magnetite in the $TiO_2$-$Fe_2O_3$-FeO system. The composition of the placer magnetites and magnetites in the volcanic rock fragments are plotted in the magmatic field in Ti-Al and Ti versus Ni/Cr diagrams. The diagrams Ti + V versus Ni/(Cr + Mn) and Ti + V versus Ca + Al + Mn indicate that placer magnetites and magnetites in the volcanic rock fragments belong to the Fe-Ti, V deposits. In the V-Ti diagram, all magnetites fall into the range of titaniferous iron ores. The comparison of the trace element composition of placer magnetites and magnetites in the volcanic rock fragments in the elemental diagrams above showed that all magnetites have the same origin, so that the placer magnetites were most likely released from the volcanic rock fragments by erosion over time. On the other hand, the comparison of the chemical composition of the volcanic rock fragments in the alluvium with that of volcanic rocks from the Ashtian area north of the Mahura deposit in the petrogenetic diagrams reveals similar nature for these rocks and that the magnetite-bearing volcanic rock fragments originate from the Ashtian Basin.

**Keywords** Placer deposit · Iron ore · Magnetite geochemistry · Provenance rocks · Mahura

## Introduction

Placer deposits are a group of sedimentary deposits consisting of an economic accumulation of some valuable heavy resistant minerals, including gold, platinum, gemstones, pyrite, magnetite, cassiterite, wolframite, rutile, monazite and zircon. These minerals are released from their source rocks by weathering and are transported and concentrated by river, wind, sea or gravity action far from or near the provenance (Morison 1989; Sutherland 1991). Depending on the means of transport and concentration, placer deposits include alluvial (transported by rivers), eolian (transported

✉ Farhad Ehya
ehya.farhad@iau.ac.ir

[1] Department of Geology, Mahallat Branch, Islamic Azad University, Mahallat, Iran

[2] Department of Geology, Behbahan Branch, Islamic Azad University, Behbahan, Iran

[3] Department of Geology, Ashtian Branch, Islamic Azad University, Ashtian, Iran

Published online: 26 July 2024

by wind), colluvial (transported by gravity), eluvial (in or near the source area) and beach placers (transported by the sea). Paleo-placers are ancient placers that have been buried and converted from the original loose sediment mass into rock (Haldar 2013). In addition to the presence of a suitable weathering environment and transportation agents, the formation of a placer deposit requires a primary source for the placer-forming minerals, which is usually crystalline rocks. Therefore, the determination of the source rock for placer minerals is of particular importance for understanding the formation conditions and the exploration of these deposits.

Iran has huge iron ore reserves as more than 200 deposits and prospects with a reserve of about 4 billion tons (Karimpour 1989). These deposits include various genetic types of Kiruna, volcano-sedimentary, skarn, iron oxide-copper-gold (IOCG), magmatic and placer deposits that occur in different Iranian tectonic zones, including Central Iran, Sanandaj-Sirjan, Zagros and Alborz zones and Urumieh-Dokhtar magmatic arc (Nabatian et al. 2015; Moinevaziri and Mirza 2021). Placer iron deposits occur in several regions of Iran, including Sangan-Khaf, Bardeskan and Ataieh areas in Khorasan-e-Razavi province (Nabatian et al. 2015; Hosseinzadeh et al. 2017; Hajalilou et al. 2021), Bazman in Sistan-va-Baluchistan province (Jahantigh and Shahraki 2014), Hamedan in Hamedan province (Badkoubeh Hazaveh and Rezaei 2021), Sangerd in Khorasan-e-Shomali province (Nourani et al. 2011), Zarnan in Zanjan province (Ebrahimi et al. 2016) and the Mahura deposit in Markazi province (Samari et al. 2014). The Sangan-Khaf placer deposits are by far the most important iron placer deposits in Iran. The literature review shows that, with the exception of a few mostly conference papers mentioned above, no comprehensive studies have been carried out on this type of iron deposit in Iran. The only study performed on the Mahura iron placer deposit includes petrological, petrographical and geochemical studies conducted by Samari et al. (2014), but a scientific and definitive conclusion on the origin of this deposit has not been provided.

The unique characteristics of magnetite, including its formation under diverse geologic conditions and the ability to host a large number of minor and trace elements in its cubic spinel structure, as well as the fact that its trace element content depends on the conditions of formation, have led to magnetite chemistry being widely used in recent years as a significant petrogenetic indicator to determine the conditions under which it was formed (e.g., Carew et al. 2006; Rusk et al. 2009; Dupuis and Beaudoin 2011; Dare et al. 2012, 2014, 2015; Nadoll et al. 2012, 2014, 2015; Hu et al. 2017; Ward et al. 2018; Ehsani Nasab and Ehya 2019; Marbouti et al. 2020; Bedard et al. 2022; Xiaoxu et al. 2023; Yi et al. 2024). In addition, the comparison of the chemical composition of magnetites found in sand beach and stream deposits with those in hard rock, e.g. from north Taiwan island (Mitwally and Yu 2022), was used to identify the magnetite's provenance. This study aims to determine the origin of magnetite based on the geochemistry of Mahura placer magnetites and magnetites in volcanic rock fragments found in alluvial deposits and to unravel the source of the volcanic rock debris based on the geochemistry of these rock fragments.

## Geological setting

### Local geology

The Mahura iron placer deposit with the geographical coordinates of 34° 16' 48" to 34° 17' 30" north latitude and 50° 03' 58" to 50° 04' 51" east longitude is located 2 km west of the Cheshmeh village and 55 km northeast of the Arak city on the eastern edge of the Meyghan Playa, in the Markazi province, Iran. The deposit area covers an area of 26 $km^2$. With regard to the sedimentary-structural subdivision of Iran, the Mahura deposit is located in the Central Iran Zone, close to the Urumieh-Dokhtar magmatic arc (Fig. 1). Based on the climate data for the city of Arak, the studied area has a mild mountain climate with cold winters and mild summers. The average annual temperature is 13.9 °C and the average annual precipitation is 341.7 mm, which is considered one of the rainiest areas in Iran.

Figure 2 shows the geological map of the Mahura deposit area. The oldest rock unit present in the deposit area consists of consolidated deposits including tuff, lapilli tuff, breccia tuff, volcanic rock fragments, conglomerate and light gray sandstone of Pliocene age. The inclination of this rock unit is low and lies at around 15° to the southwest. The second Pliocene rock unit, which overlies the previous one, contains consolidated and unconsolidated dark to gray-colored conglomerates with a sandy matrix, containing fragments and blocks of volcanic rock up to 50 cm long with andesite and microdiorite composition from the late Neogene. Ghadimi and Esmaeli (2022) gave the components of this rock unit in order of occurrence as sandstone (45%), andesite (37%), limestone (7%), tuff (5%), rhyolite (3%) and chert fragments and basalt (3%). These rock components originate from the erosion of the lower Pliocene unit as well as from conglomerate, sandstone, limestone and various volcanic rocks from neighboring areas, especially from the Ashtian Basin in the north of the study area (Ghadimi and Esmaeli 2022). The Pliocene rock units are about 500 m thick in total.

The youngest deposits in the study area are Quaternary alluvial deposits, including young terraces and gravelly fans, consisting of cream to earthy-colored sandy, silty and clayey sediments and volcanic rock fragments formed by

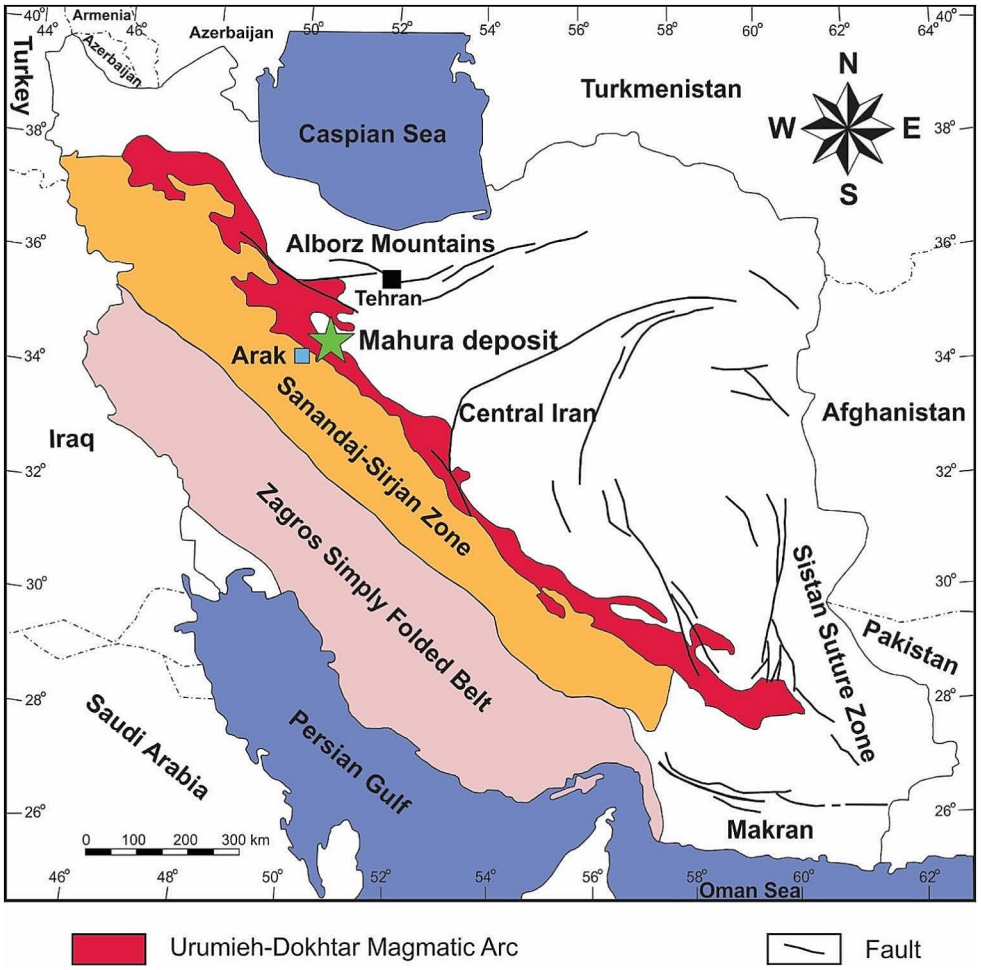


**Fig. 1** Main tectonic zones of Iran and location of the Mahura iron placer deposit (modified after Ghasemi and Talbot 2006)

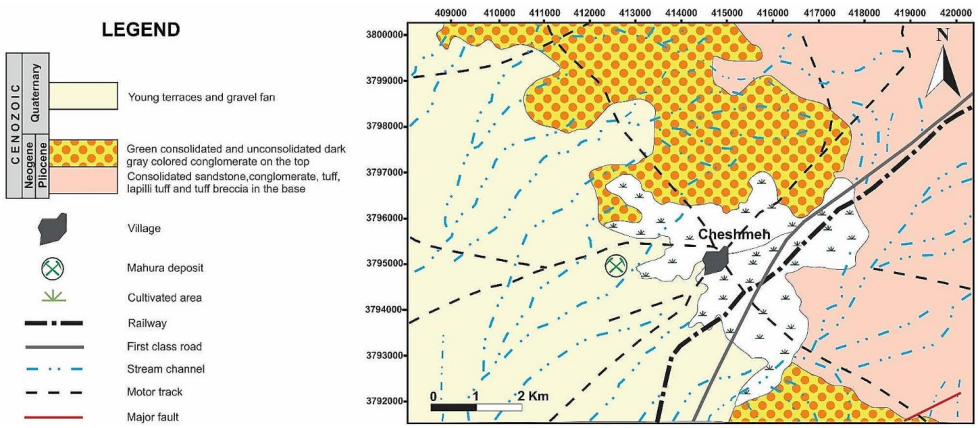


**Fig. 2** Simplified geologic map of the Mahura area (modified after Alai Mahabadi 2000)

erosion of older deposits, particularly old alluvial deposits. The Mahura iron placer deposit occurs in this Quaternary alluvium (Figs. 2 and 3a). In the walls of the mining trenches, signs of stream sedimentation such as irregularly graded bedding, current orientation of the sediments and indications of the change from flood currents to slow ones and vice versa can be easily observed. The area where the iron placer deposit is located is a vast plain with an extension of several square kilometers, bordered on sides by the heights of the area. Considering the extent of the plain and the lack of outcrops of geological units, it can be said that the thickness of the accumulated alluvium in this plain is high, reaching more than 100 m in some places. Numerous seasonal rivers flow from the mountain slopes and cut through the plain in a network. The length of these channels varies from a few kilometers to several tens of kilometers, and their


**Fig. 3** (**a**) Photograph showing the Quaternary alluvium where the Mahura iron placer deposit occurs; (**b**) Photograph showing one of the pits dug into the alluvium to extract the ore; (**c**) and (**d**) Photographs showing the equipment at the Mahura mine used for screening and processing the ore after mining

width varies from a few meters to several tens of meters. As the deposit area is covered by young rock units and alluvial deposits, it lacks significant structural features with the exception of a fault on the southeastern edge (Fig. 2).

### Mineralization style

Exploration work in the Mahura area began in 2009 and the mine was commissioned in 2013. The iron mineralization in the Mahura area occurs in the form of placer deposits in the Quaternary alluvium. The placer minerals include micrometer-sized grains of magnetite and titanomagnetite, whose black color shows how they are distributed in the alluvium. The grade measurements show that the average $Fe_2O_3$ content is around 7%. The proved reserve is 1,980,000 tons, while the probable reserve is estimated around 10 million tons (IMIMT, 2012). The ore is extracted from open pits dug into the alluvial deposits (Fig. 3b). After the ore is passed through the magnetic separation plant at the mine site (Fig. 3c and d), the ore grade reaches around 50% $Fe_2O_3$. The $TiO_2$ content of the ore is high, up to 11–12%.

## Samples and methods

Fifty-six samples of alluvium and volcanic rock fragments found in the alluvium were collected from intact alluvium and mining trenches during field observations to carry out petrographic and geochemical studies. For petrographic studies, thirteen thin and polished-thin sections were prepared from samples of volcanic rock fragments in the laboratory of Iranian Mineral Processing Research Center (IMPRC), Karaj, Iran, and examined using transmission/reflection polarizing microscope in the petrographic laboratories of Mahallat Islamic Azad University, Mahallat, Iran, and Geological Survey of Iran, Tehran.

To study the mineralogy of the placers, seven samples were taken from the alluvial sediments at a depth of 15–20 cm and analyzed for heavy minerals. The selected samples were analyzed in the heavy minerals laboratory of the Geological Survey of Iran in Tehran. After panning, the samples were immersed in a heavy bromoform liquid with a specific gravity of 2.87 gr/cm$^3$ to separate the heavy minerals from the light minerals. The heavy minerals extracted from the liquid were dried and then separated using a magnetic

separator. The magnetically separated phases were examined microscopically using a binocular microscope.

To determine the geochemistry of placer magnetites, five ore samples were selected from places where magnetite had been separated and concentrated from alluvium by seasonal rainfall. The magnetites were first separated with a magnet and dried after careful washing by diluted HCl and distilled water, and then analyzed in the IMPRC using ICP-MS method. For the major elements, the detection limit is 0.01%. The detection limit is 0.1 ppm for Be, Ta, Eu, Tb, Dy, Ho, Er and Lu, whereas it is 1.0 ppm for other trace elements and rare earths. The measurement uncertainty was achieved at a confidence interval of 95% with a coverage factor of k = 2 using standard materials.

Thirteen samples of fresh volcanic rock fragments present in the alluvium were analyzed for trace and rare earth elements using ICP-MS method at the IMPRC and thirteen samples were analyzed for major oxides by XRF method at Kansaran Binaloud Company laboratory, Tehran, Iran. The detection limit of the ICP-MS analysis is 1 ppm for Zr, La, Ce, Pr, Nd, Sm, Gd, Tm and Yb, while it is 0.1 ppm for Eu, Tb, Dy, Ho, Er and Lu. The detection limit is 0.01% for all the major oxides analyzed with the XRF method. The measurement uncertainty for the ICP-MS and XRF methods was achieved with a confidence interval of 95% and a coverage factor of k = 2 using standard materials.

To investigate the chemistry of magnetite in fresh volcanic rock fragments, five polished-thin sections were prepared from these rocks and analyzed at twenty magnetite points using an electron probe microanalyzer (EPMA), model Cameca SX100, at the IMPRC. The analysis was done with a beam of 2–5 μ diameter at a voltage of 15 Kev and a current of 20 nA. Precision for electron probe analysis was generally better than ± 2%.

## Results

### Petrography of the volcanic rock fragments

The volcanic rock fragments are green, brown, light to dark gray and black in hand specimens (Fig. 4). Some samples have a vesicular appearance, as the cavities are filled in places by secondary minerals such as calcite, chlorite and quartz, forming an amygdaloidal structure. The cavities are mostly spherical and sometimes oval. Based on the type and modal percentage of minerals and the textural relationships, the volcanic rock fragments have been identified as andesite and basaltic andesite. Microscopic studies revealed that the texture of these rocks is porphyritic and contains phenocrysts of plagioclase, amphibole and pyroxene in a microcrystalline matrix. The matrix consists of microcrystals of plagioclase, quartz and glass, which together make up 35–40% of the rock. Plagioclase is observed in the form of phenocrysts with an abundance of 20 to 45% and a size of about 0.1 to 3 mm. Plagioclase is mostly euhedral to subhedral and exhibits polysynthetic and Carlsbad twinning and in some cases zoning (Fig. 5a and b). Amphibole and pyroxene are also found as phenocrysts with an abundance of 4 to 12% and sizes of 0.2 to 1.5 mm (Fig. 5a, b, c and d). In general, pyroxene crystals are less common than amphibole and in some cases altered to amphibole. The volcanic rocks are affected by alteration in places as their phenocrysts and groundmass transform into alteration products such as calcite, chlorite, sericite, clay minerals and iron oxides and hydroxides (Fig. 5d). Magnetite with disseminated texture is observed in the groundmass and as inclusions in plagioclase and amphibole crystals (Fig. 5e). The abundance of magnetite is about 4 to 10%, with a variable size of 0.1 to 0.4 mm. Magnetite has been transformed in fractures into hematite by martitization and sometimes into goethite due to intense oxidation (Fig. 5f). Apatite is rarely observed as fine inclusions in amphibole and plagioclase crystals.

### Heavy mineral studies

The results of the heavy mineral analyses are provided in Table 1. Magnetite is the most abundant mineral in the analyzed samples with an average abundance of 48.8 vol%. Pyroxene and altered minerals are the next most abundant minerals with an average abundance of 21.7 and 20.7 vol%, respectively. Hematite and epidote have an average abundance of 4.1 and 2.0 vol%, respectively, followed by limonite, ilmenite, amphibole, barite, pyrite oxide, zircon, celestine, apatite, rutile and carbonates with average abundances of < 1.0 to 0.0 vol%. Barite and celestine probably originate from the evaporation of alluvium pore waters and/or evaporite sediments from the Meyghan Playa. While altered minerals, epidote, hematite and limonite are derived from the alteration of ferromagnesium minerals, other minerals are possibly the result of liberation from the rocks containing them through weathering. The origin of magnetite is discussed below.

### Chemistry of magnetite

#### Placer magnetites

The concentrations of major and some trace elements in five placer magnetite samples from the Mahura deposit analyzed by the ICP-MS method are given in Table 2. The concentration of Fe varies from 60.6 to 63.3% in magnetite samples. The elements Mg, Al, Ti, Ca and Na have the highest concentrations in magnetites. Magnesium and Ti are

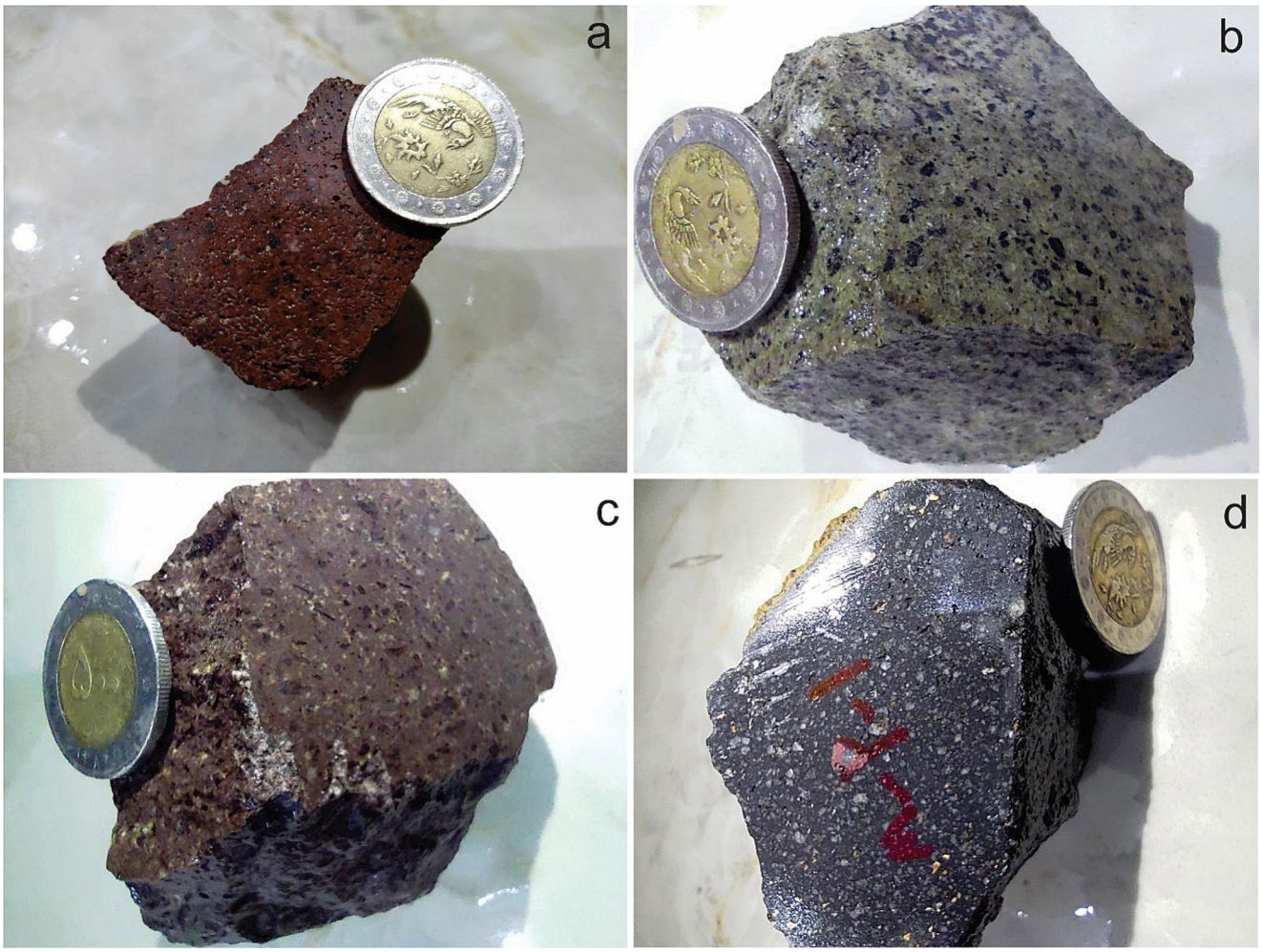


**Fig. 4** Hand specimens of volcanic rock fragments from the Mahura iron placer deposit. (**a**) Photograph showing a brown vesicular andesite sample; (**b**) Photograph showing a gray basaltic andesite sample; (**c**) Photograph showing a brown basaltic andesite sample; and (d) Photograph showing a gray vesicular andesite sample

compatible in the magnetite structure, while Na, Al and Ca are incompatible (Dare et al. 2014). The concentration of Mg and Ti (2.53–3.86%) in Mahura placer magnetites is also higher than the concentration of Na, Al and Ca (0.21–2.95%). The lowest values (< 100 ppm) for trace elements belong to Ag, As, Be, Ga, Mo, Nb, Ni, Pb, Rb, Sc, Y, Zn and Ta, whereas the highest (> 100 ppm) are found for Ba, Co, Cr, Cu, Mn, V, Zr and Sr. Nickel, Co, Cr, V and Mn are among the compatible elements in the magnetite structure. The amounts of rare earth elements (REEs) in the magnetite samples are very low, so that with the exception of La, Ce, Dy and Er in some samples, the concentration of the other REEs in all samples is below the detection limits of 0.1 and 1 ppm (Table 2).

## Magnetites in the volcanic rock fragments

The results of the chemical analysis of magnetite in volcanic rock fragments using the EPMA method as well as calculations of the structural formula of magnetite based on 32 oxygen atoms and 24 cations are given in Table 3. The concentration of FeO in the samples is between 72.47 and 80.89%. The concentrations of $Cr_2O_3$ and NiO are less than 1%, except for NiO, which accounts for almost 1% in two points. The amount of $TiO_2$ varies between 5.48 and 12.18%, indicating a high Ti content in the composition of the magnetite and the formation of titanomagnetite. The concentration of $Al_2O_3$ is low (1.57–3.95%), which shows that spinel does not form in the samples. The $V_2O_3$ content is in the range of 0.56–2.23%. The $SiO_2$ content ranges from 0 to 2.97%, the MnO content from 0 to 1.66%, the MgO content from 0.17 to 2.96%, the CaO content from 0

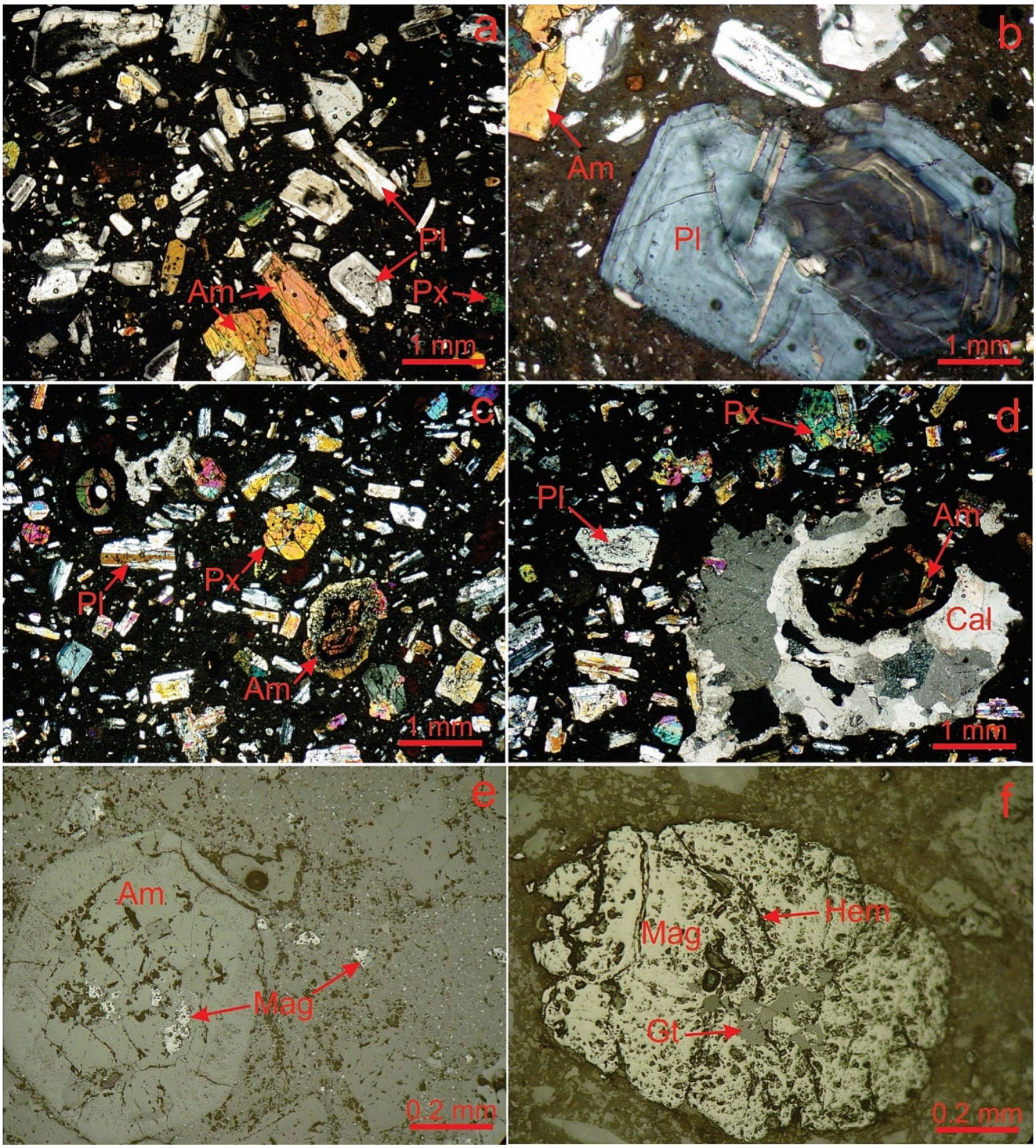


**Fig. 5** Photomicrographs of the volcanic rock fragments from the Mahura iron placer deposit. (**a**) Plagioclase phenocrysts with polysynthetic twinning and zoning together with amphibole and traces of pyroxene in a microcrystalline to glassy matrix of an andesite; (**b**) A large zoned plagioclase phenocryst together with amphibole in a microcrystalline to glassy matrix of an andesite; (**c**) Phenocrysts of plagioclase, amphibole and pyroxene in a microcrystalline to glassy matrix of a basaltic andesite; (**d**) The cavities in a microcrystalline to glassy matrix of a basaltic andesite with plagioclase, amphibole and pyroxene phenocrysts filled by calcite; (**e**) Magnetite inclusions in an amphibole phenocryst and in the groundmass; and (**f**) Alteration and oxidation of magnetite to hematite (martitization) and goethite. Photomicrographs a to d in XPL, e and f in PPL. Am = amphibole, Pl = plagioclase, Px = pyroxene, Cal = calcite, Mag = magnetite, Hem = hematite, Gt = Goethite

**Table 1** Frequency of minerals detected in the alluvium samples subjected to heavy mineral analyses (vol%)

| Minerals | HM-1 | HM-2 | HM-3 | HM-4 | HM-5 | HM-6 | HM-7 | Average |
|---|---|---|---|---|---|---|---|---|
| **Magnetite** | 58.5 | 72.0 | 31.5 | 36.0 | 63.0 | 63.0 | 18.0 | 48.8 |
| **Hematite** | 3.0 | 2.0 | 6.5 | 9.0 | 1.5 | 3.0 | 4.0 | 4.1 |
| **Ilmenite** | 0.6 | 0.4 | 0.6 | 0.0 | 0.0 | 0.3 | 0.8 | 0.4 |
| **Pyroxene** | 15.0 | 8.0 | 35.7 | 21.0 | 13.5 | 15.0 | 44.0 | 21.7 |
| **Amphibole** | 0.3 | 0.1 | 0.1 | 0.3 | 0.3 | 0.6 | 0.8 | 0.3 |
| **Epidote** | 1.5 | 1.0 | 0.1 | 3.0 | 3.0 | 1.5 | 4.0 | 2.0 |
| **Pyrite oxide** | 0.3 | 0.2 | 0.6 | 0.3 | 0.3 | 0.0 | 0.0 | 0.2 |
| **Limonite** | 1.5 | 0.2 | 0.6 | 0.6 | 1.5 | 0.6 | 1.6 | 0.9 |
| **Zircon** | 1.0 | 0.0 | 0.1 | 0.1 | 0.1 | 0.1 | 0.1 | 0.2 |
| **Apatite** | 0.2 | 0.0 | 0.0 | 0.0 | 0.0 | 0.0 | 0.0 | 0.0 |
| **Rutile** | 0.2 | 0.0 | 0.0 | 0.0 | 0.0 | 0.0 | 0.0 | 0.0 |
| **Barite** | 1.5 | 0.0 | 0.0 | 0.0 | 0.1 | 0.1 | 0.3 | 0.3 |
| **Celestine** | 0.5 | 0.0 | 0.0 | 0.0 | 0.1 | 0.4 | 0.0 | 0.1 |
| **Carbonates** | 0.2 | 0.0 | 0.0 | 0.0 | 0.0 | 0.1 | 0.1 | 0.0 |
| **Altered minerals** | 15.5 | 16.0 | 26.2 | 28.0 | 17.5 | 16.1 | 26.0 | 20.7 |
| **Total** | 99.8 | 99.9 | 102.0 | 98.3 | 100.9 | 100.8 | 99.7 | 100.2 |

to 0.45%, the $Na_2O$ content from 0 to 0.01%, and the $K_2O$ content from 0 to 0.02% (Table 3).

### Chemical composition of the volcanic rock fragments

The contents of major and rare earth elements in thirteen samples of volcanic rock fragments found in the alluvium of the Mahura area are listed in Table 4. The $SiO_2$ content of the samples ranges from 57.37 to 63.33%, indicating that the volcanic rocks are intermediate in composition. The $Al_2O_3$ and $Fe_2O_3$ contents range from 17.55 to 19.13% and from 4.80 to 7.21%, respectively. The concentrations of the alkaline earth metal oxides CaO and MgO range from 5.73 to 9.53% and from 2.07 to 4.49%, respectively. The $Na_2O$ content is between 2.01 and 2.63%, $K_2O$ content between 0.22 and 2.43%. The $TiO_2$, MnO and $P_2O_5$ contents are in the range of 0.50–0.87%, 0.04–0.16% and 0.08–0.40%, respectively. The LOI content of the samples is between 0.77 and 3.53%. The concentration of the trace element Zr ranges from 104.06 to 240.00 ppm. The total concentration of rare earth elements (ΣREE) in the samples ranges from 7.31 to 39.78 ppm.

## Discussion

### Type of magnetite

The triangular diagram $TiO_2$-FeO-$Fe_2O_3$ is used to identify the type of magnetite in the volcanic rock fragments from the Mahura area (Buddington and Lindsley 1964) (Fig. 6). As it was not possible to analyze the placer magnetites with the EPMA method, but they were analyzed using the ICP-MS method, the amounts of bivalent and trivalent Fe in these samples are not known, so they cannot be plotted in the diagram above. The magnetite samples in the volcanic rock fragments are located along the magnetite-ulvospinel line (titanomagnetite) with a tendency towards magnetite. This is clearly due to the high Ti content in the magnetite structure. The high Ti content in placer magnetites (2.59–3.33%; Table 2) also indicates the presence of titanomagnetite. Confirming this conclusion, magnetite and titanomagnetite minerals were observed in the SEM-BSE images of the volcanic rock fragments (Fig. 7). The EPMA analyses also revealed some small parts in the magnetite where magnetite was intergrown with ilmenite. This is indicated by the high concentration of Ti in some of the points analyzed (Table 3). Such textures are common in magmatic magnetite due to the high formation temperature and high Ti content, while they are rare in hydrothermal magnetite (Ray and Webster 2007). The magma emplacement in the upper parts of the crust can increase oxygen fugacity due to degassing from the melt and the removal of ferrous iron by secondary fluids during cooling. The increase in oxygen fugacity reduces the solubility of Ti in magnetite and leads to the formation of ilmenite exsolution lamellae and inclusions according to the following equation (Bell and Simon 2011; Dilles et al. 2015):

$$6Fe_2TiO_4 + O_2 \rightarrow 6FeTiO_3 + 2Fe_3O_4$$

### Magnetite provenance rocks

Magnetite has an inverse spinel structure with the general formula $AB_2O_4$, where A is occupied by divalent cations such as Mg, Mn, Zn, Co and Ni and B by trivalent cations

**Table 2** The concentrations of major and some trace elements in placer magnetite samples (analyzed by the ICP-MS method) from the Mahura deposit

| Sample No. | Mahmeg-01 | Mahmeg-04 | Mahmeg-05 | Mahmeg-07 | Mahmeg-11 |
|---|---|---|---|---|---|
| Major elements (%) | | | | | |
| **Fe** | 61.6 | 63.3 | 61.7 | 60.6 | 61.5 |
| **Al** | 2.70 | 2.08 | 2.35 | 2.95 | 2.86 |
| **Ca** | 1.45 | 0.89 | 1.24 | 1.88 | 1.64 |
| **Mg** | 3.29 | 2.53 | 3.31 | 3.86 | 3.12 |
| **Na** | 0.40 | 0.21 | 0.31 | 0.45 | 0.41 |
| **Ti** | 2.87 | 3.30 | 3.33 | 2.59 | 2.80 |
| **Trace elements (ppm)** | | | | | |
| **Ag** | 2.67 | 2.24 | 2.8 | < 1 | 2.31 |
| **As** | 4.89 | 3.3 | < 1 | < 1 | 3.55 |
| **Ba** | 422 | 133 | 80 | 108 | 104 |
| **Be** | < 0.1 | 0.29 | < 0.1 | < 0.1 | < 0.1 |
| **Co** | 147 | 161 | 158 | 130 | 140 |
| **Cr** | 274 | 258 | 281 | 204 | 256 |
| **V** | 158 | 139 | 208 | 93 | 138 |
| **Cu** | 1365 | 276 | 76 | 114 | 70 |
| **Zn** | 139 | 84 | 80 | 66 | 61 |
| **Zr** | 107 | 145 | 143 | 104 | 129 |
| **Ga** | 8.14 | 7.99 | 8.04 | 6.11 | 7.84 |
| **Mn** | 2878 | 2992 | 3219 | 2808 | 2957 |
| **Mo** | 4.97 | 1.11 | 1.14 | 0.57 | 0.77 |
| **Nb** | 3.34 | 3.12 | 3.66 | 2.42 | 3.18 |
| **Ni** | 49.89 | 54.48 | 48.75 | 44.8 | 50.28 |
| **Pb** | 45.77 | 42.76 | 33.12 | 27.38 | 42.89 |
| **Rb** | 1.29 | < 1 | < 1 | < 1 | < 1 |
| **Sc** | 5.65 | 3.47 | 7.72 | 6.24 | 6.39 |
| **Sr** | 198 | 114 | 99 | 162 | 204 |
| **Ta** | 0.18 | 0.16 | 0.18 | 0.14 | 0.18 |
| **Y** | < 1 | < 1 | < 1 | 3.48 | < 1 |
| **Ni/Cr** | 0.18 | 0.21 | 0.17 | 0.22 | 0.19 |
| **Rare earth elements (ppm)** | | | | | |
| **La** | 1.78 | 1.77 | 1.55 | 3.79 | 1.72 |
| **Ce** | < 1 | < 1 | < 1 | 2.01 | < 1 |
| **Pr** | < 1 | < 1 | < 1 | < 1 | < 1 |
| **Sm** | < 1 | < 1 | < 1 | < 1 | < 1 |
| **Eu** | < 0.1 | < 0.1 | < 0.1 | < 0.1 | < 0.1 |
| **Gd** | < 1 | < 1 | < 1 | < 1 | < 1 |
| **Tb** | < 0.1 | < 0.1 | < 0.1 | < 0.1 | < 0.1 |
| **Dy** | 0.34 | 0.13 | 0.28 | 0.28 | 0.38 |
| **Ho** | < 0.1 | < 0.1 | < 0.1 | < 0.1 | < 0.1 |
| **Er** | 0.18 | < 0.1 | 0.16 | 0.19 | 0.14 |
| **Tm** | < 1 | < 1 | < 1 | < 1 | < 1 |
| **Yb** | < 1 | < 1 | < 1 | < 1 | < 1 |
| **Lu** | < 0.1 | < 0.1 | < 0.1 | < 0.1 | < 0.1 |

such as Al, Ga and As (Nadoll et al. 2014). Tetravalent ions such as $Ti^{+4}$ can also occupy the position of $Fe^{+3}$ by double substitution with a divalent cation (Wechsler et al. 1984). Vanadium, Cr and Mn have different valences and their participation in the magnetite structure depends on the oxygen fugacity (Sievwright et al. 2017; Sossi et al. 2018). In general, the type and concentration of trace elements in magnetite depend on the physicochemical parameters of the magnetite-forming system, such as temperature, $fO_2$, XSi (silica activity), ionic radii similarities, cation valences, fluid/melt composition, host rock buffer and re-equilibration processes (Nadoll et al. 2012, 2014; Dare et al. 2014; Buddington and Lindsley 1964; Lindsley 1991; Toplis and Carroll 1995; Chen et al. 2015). This property has led to the chemical composition of magnetite being used as an indicator of the type of iron oxide deposits (Carew et al. 2006; Singoyi et al. 2006; Rusk et al. 2009; Dupuis and Beaudoin 2011; Zhang et al. 2011; Nadoll et al. 2012). Moreover, several compositional diagrams using minor and trace elements of magnetite are recently proposed to better understand the origin of iron oxide deposits in different mineralizing systems (Dupuis and Beaudoin 2011; Nadoll et al. 2014; Dare et al. 2014). Magnetite is formed from hydrothermal fluids at low temperatures to produce large hydrothermal magnetite deposits (Bookstrom 1995; Groves et al. 2010; Nadoll et al. 2012). It can also be crystallized from sulfide and silicate melts at high temperature (Dare et al. 2014). When magnetite crystallizes from silicate melts, it is usually enriched in lithophile elements such as Ti, Cr, V, Al, Mn, Ca, Nb, Ga, Ta, Hf and Zr, while the concentration of chalcophile elements such as Ni, Co, Sc and Pb is high in magnetites deposited from sulfide-rich fluids (Cygan and Candela 1995; Toplis and Corgne 2002; Simon et al. 2008; Dare et al. 2014). Hydrothermal magnetite has low concentrations of Si and Ga and a high content of Mg (Hu et al. 2014; Nadoll et al. 2014; Heidarian et al. 2017). Magnetite with low concentrations of Ti, Cr, V, Ni and Mn can be formed through the metamorphism of sulfides (Boutroy et al. 2014).

The Mn content of 50 to 400 ppm is an indicator of hydrothermal magnetites, while Mn concentrations between 102 and 12,500 ppm are characteristic of magmatic (igneous) magnetites (Nadoll et al. 2014). With the exception of one spot in magnetites from the volcanic rock fragments, where the Mn content is 0%, the Mn concentration in Mahura placer magnetites and magnetites in volcanic rock fragments is in the ranges of 2808–3219 ppm and 0.02–0.43%, respectively (Tables 2 and 3), consistent with the magmatic origin of magnetite. Most hydrothermal magnetites have a Ti content of less than 2% and an Al content of less than 1% (Hu et al. 2014). The contents of Ti and V in magnetite is strongly controlled by the oxygen fugacity (Toplis and Corgne 2002). The Ti and Al contents in placer magnetites (2.59–3.33% and 2.08–2.95%, respectively; Table 2) are above 2%, revealing a magmatic origin of these magnetites. In magnetites from the volcanic rock fragments, although the Ti concentration is below 2% (1.22–2.74%) and the

**Table 3** The concentrations of major and some trace elements in magnetite (analyzed by the EPMA method) from volcanic rock fragments

| Sample no | 1-pet5 | 2-pet5 | 3-pet5 | 4-pet5 | 5-pet9 | 6-pet9 | 7-pet9 | 8-pet9 | 9-pet6 | 10-pet6 | 11-pet6 |
|---|---|---|---|---|---|---|---|---|---|---|---|
| **$SiO_2$** | 0.25 | 0.27 | 0.14 | 0.1 | 0.07 | 0.1 | 0.06 | 0.35 | 1.34 | 2.97 | 0.01 |
| **$TiO_2$** | 12.18 | 10.42 | 6.25 | 10.73 | 6.66 | 7.37 | 7.66 | 7.55 | 11.03 | 11.65 | 10.85 |
| **$Al_2O_3$** | 3.02 | 3.43 | 3.95 | 2.63 | 1.74 | 1.85 | 1.75 | 1.57 | 2.5 | 2.71 | 2.01 |
| **$Cr_2O_3$** | 0.41 | 0.41 | 0.07 | 0.24 | 0.1 | 0.14 | 0.1 | 0.12 | 0.21 | 0.19 | 0.15 |
| **$V_2O_3$** | 1.19 | 1.05 | 1.65 | 1.09 | 0.56 | 0.75 | 0.56 | 0.78 | 1.17 | 1.18 | 1.18 |
| **FeO** | 74.88 | 75.57 | 78.54 | 74.2 | 79.26 | 79.48 | 79.49 | 79.24 | 75.92 | 72.47 | 78.33 |
| **MnO** | 0.46 | 0.38 | 0.62 | 0.31 | 0.44 | 0.38 | 0.5 | 0.41 | 0.43 | 0.23 | 0.42 |
| **MgO** | 2.76 | 2.96 | 1.27 | 2.16 | 1.37 | 1.47 | 1.36 | 1.24 | 0.43 | 0.17 | 1.45 |
| **CaO** | 0.19 | 0.05 | 0.32 | 0.1 | 0 | 0 | 0 | 0.04 | 0.18 | 0.45 | 0 |
| **$Na_2O$** | 0 | 0 | 0 | 0 | 0.05 | 0 | 0 | 0.16 | 0.04 | 0 | 0 |
| **$K_2O$** | 0 | 0.21 | 0.7 | 0 | 0 | 0.09 | 0 | 0 | 0 | 0.02 | 0 |
| **NiO** | 0 | 0 | 0.15 | 0 | 0.65 | 0 | 0 | 0 | 0.27 | 0 | 0.12 |
| **Fe/(Fe + Mg)** | 0.94 | 0.93 | 0.93 | 0.87 | 0.97 | 0.97 | 0.97 | 0.97 | 0.99 | 0.99 | 0.97 |
| **Cr/(Cr + Al)** | 0.08 | 0.07 | 0.01 | 0.06 | 0.04 | 0.05 | 0.04 | 0.05 | 0.05 | 0.04 | 0.05 |
| **$Fe^{+2}$** | 9.40 | 9.01 | 7.76 | 7.60 | 8.68 | 8.98 | 9.05 | 9.21 | 10.54 | 11.38 | 9.69 |
| **$Fe^{+3}$** | 9.24 | 9.82 | 11.62 | 10.32 | 12.12 | 11.75 | 11.7 | 11.56 | 9.07 | 7.60 | 10.26 |
| **$Fe^{+2}/(Fe^{+2}+Fe^{+3})$** | 0.50 | 0.48 | 0.40 | 0.42 | 0.41 | 0.43 | 0.43 | 0.44 | 0.54 | 0.60 | 0.48 |
| **$Fe^{+3}/(Fe^{+3}+Fe^{+2})$** | 0.49 | 0.52 | 0.60 | 0.57 | 0.58 | 0.56 | 0.56 | 0.55 | 0.46 | 0.40 | 0.51 |
| **Si** | 0.07 | 0.08 | 0.04 | 0.03 | 0.02 | 0.03 | 0.02 | 0.11 | 0.41 | 0.93 | 0 |
| **Ti** | 2.73 | 2.33 | 1.39 | 2.33 | 1.57 | 1.73 | 1.80 | 1.78 | 2.56 | 2.74 | 2.48 |
| **Al** | 1.06 | 1.20 | 1.37 | 0.89 | 0.64 | 0.68 | 0.64 | 0.58 | 0.91 | 1.00 | 0.72 |
| **Cr** | 0.09 | 0.09 | 0.01 | 0.05 | 0.02 | 0.03 | 0.02 | 0.03 | 0.05 | 0.04 | 0.03 |
| **V** | 0.81 | 0.71 | 1.12 | 0.74 | 0.38 | 0.51 | 0.38 | 0.53 | 0.79 | 0.80 | 0.80 |
| **Mn** | 0.11 | 0.09 | 0.15 | 0.07 | 0.12 | 0.10 | 0.13 | 0.11 | 0.11 | 0.06 | 0.11 |
| **Mg** | 1.22 | 1.31 | 1.44 | 2.65 | 0.64 | 0.68 | 0.63 | 0.58 | 0.20 | 0.08 | 0.66 |
| **Ca** | 0.06 | 0.01 | 0.10 | 0.03 | 0 | 0 | 0 | 0.01 | 0.06 | 0.15 | 0 |
| **Na** | 0 | 0 | 0 | 0 | 0.01 | 0 | 0 | 0.02 | 0.01 | 0 | 0 |
| **K** | 0 | 0.02 | 0.06 | 0 | 0 | 0.01 | 0 | 0 | 0 | 0 | 0 |
| **Ni** | 0 | 0 | 0.03 | 0 | 0.16 | 0 | 0 | 0 | 0.06 | 0 | 0.03 |
| **Ni/Cr** | 0 | 0 | 3 | 0 | 8 | 0 | 0 | 0 | 1.2 | 0 | 1 |
| **Sample no** | **11-pet6** | **12-pet6** | **13-pet6** | **14-pet6** | **15-pet6** | **16-pet9** | **17-pet9** | **18-pet9** | **19-pet9** | | |
| **$SiO_2$** | 0.34 | 0 | 1.26 | 0.99 | 0.19 | 0 | 0.8 | 0.52 | 0 | | |
| **$TiO_2$** | 9.66 | 10.09 | 11.5 | 10.38 | 10.32 | 7.23 | 5.48 | 7.99 | 8.09 | | |
| **$Al_2O_3$** | 2.94 | 2.98 | 2.75 | 3.24 | 3.44 | 2.97 | 5.26 | 3.27 | 2.84 | | |
| **$Cr_2O_3$** | 0.19 | 0.2 | 0.18 | 0.15 | 0.08 | 0.07 | 0.15 | 0.05 | 0.08 | | |
| **$V_2O_3$** | 0.99 | 0.97 | 1.15 | 1.24 | 1.01 | 0.74 | 0.74 | 0.85 | 2.23 | | |
| **FeO** | 74.46 | 76.27 | 74.06 | 73.39 | 73.12 | 79.23 | 80.54 | 80.3 | 80.89 | | |
| **MnO** | 1.66 | 0.38 | 0.45 | 0.44 | 1.11 | 0.46 | 0.27 | 0 | 0.09 | | |
| **MgO** | 1.71 | 1.81 | 1.64 | 1.94 | 2.18 | 1.18 | 1.25 | 0.95 | 0.96 | | |
| **CaO** | 0 | 0 | 0.06 | 0.11 | 0 | 0 | 0 | 0 | 0.09 | | |
| **$Na_2O$** | 0 | 0 | 0.01 | 0.02 | 0.07 | 0.13 | 0 | 0.04 | 0.14 | | |
| **$K_2O$** | 0 | 0 | 0 | 0.04 | 0.03 | 0 | 0 | 0 | 0 | | |
| **NiO** | 0 | 0 | 1.02 | 1.16 | 0.51 | 0.86 | 0 | 0.61 | 0 | | |
| **Fe/(Fe + Mg)** | 0.96 | 0.96 | 0.96 | 0.95 | 0.95 | 0.97 | 0.97 | 0.98 | 0.98 | | |
| **Cr/(Cr + Al)** | 0.04 | 0.04 | 0.04 | 0.03 | 0.01 | 0.01 | 0.02 | 0.01 | 0.02 | | |
| **$Fe^{+2}$** | 9.13 | 9.40 | 9.88 | 9.37 | 9.04 | 8.82 | 8.84 | 9.40 | 9.38 | | |
| **$Fe^{+3}$** | 10.16 | 10.20 | 8.94 | 9.39 | 9.80 | 11.53 | 11.19 | 10.87 | 11.21 | | |
| **$Fe^{+2}/(Fe^{+2}+Fe^{+3})$** | 0.47 | 0.48 | 0.52 | 0.50 | 0.48 | 0.43 | 0.44 | 0.46 | 0.45 | | |
| **$Fe^{+3}/(Fe^{+3}+Fe^{+2})$** | 0.52 | 0.52 | 0.47 | 0.50 | 0.52 | 0.56 | 0.56 | 0.53 | 0.54 | | |
| **Si** | 0.10 | 0 | 0.38 | 0.30 | 0.06 | 0 | 0.24 | 0.15 | 0 | | |
| **Ti** | 2.25 | 2.33 | 2.63 | 2.39 | 2.39 | 1.67 | 1.22 | 1.81 | 1.85 | | |
| **Al** | 1.07 | 1.08 | 0.98 | 1.16 | 1.25 | 1.07 | 1.84 | 1.16 | 1.02 | | |
| **Cr** | 0.04 | 0.05 | 0.04 | 0.03 | 0.02 | 0.02 | 0.03 | 0.01 | 0.02 | | |
| **V** | 0.67 | 0.66 | 0.78 | 0.84 | 0.68 | 0.50 | 0.50 | 0.58 | 1.51 | | |

**Table 3** (continued)

| Sample no | 1-pet5 | 2-pet5 | 3-pet5 | 4-pet5 | 5-pet9 | 6-pet9 | 7-pet9 | 8-pet9 | 9-pet6 | 10-pet6 | 11-pet6 |
|---|---|---|---|---|---|---|---|---|---|---|---|
| **Mn** | 0.43 | 0.10 | 0.11 | 0.11 | 0.29 | 0.12 | 0.07 | 0 | 0.02 | | |
| **Mg** | 0.79 | 0.83 | 0.74 | 0.88 | 1.00 | 0.54 | 0.55 | 0.43 | 0.43 | | |
| **Ca** | 0 | 0 | 0.02 | 0.03 | 0 | 0 | 0 | 0 | 0.03 | | |
| **Na** | 0 | 0 | 0 | 0 | 0.01 | 0.02 | 0 | 0.01 | 0.02 | | |
| **K** | 0 | 0 | 0 | 0 | 0 | 0 | 0 | 0 | 0 | | |
| **Ni** | 0 | 0 | 0.25 | 0.28 | 0.12 | 0.21 | 0 | 0.15 | 0 | | |
| **Ni/Cr** | 0 | 0 | 6.25 | 9.33 | 6 | 10.5 | 0 | 15 | 0 | | |

**Table 4** The concentrations of major (analyzed by the XRF method) and rare earth elements (analyzed by the ICP-MS method) in samples of volcanic rock fragments

| Sample | Mah-pet-10 | Mah-pet-17-01 | Mah-pet-17-02 | Mah-pet-15 | Mah-pet-13 | Mah-pet-2 | Mah-pet-7 | Mah-pet-5 | Mah-pet-3 | Mah-pet-9 | Mah-pet-6 | Mah-pet-1 | Mah-pet-4 |
|---|---|---|---|---|---|---|---|---|---|---|---|---|---|
| | Major elements (%) | | | | | | | | | | | | |
| **$SiO_2$** | 62.42 | 57.46 | 61.85 | 57.48 | 58.23 | 61.84 | 59.11 | 57.37 | 60.93 | 62.35 | 59.65 | 62.87 | 63.33 |
| **$Al_2O_3$** | 17.56 | 19.13 | 18.61 | 17.55 | 18.15 | 18.56 | 17.97 | 18.98 | 18.89 | 18.32 | 19.02 | 18.04 | 17.91 |
| **$Fe_2O_3$** | 5.00 | 6.26 | 5.88 | 7.21 | 6.77 | 4.94 | 5.84 | 6.48 | 5.73 | 5.55 | 6.29 | 4.80 | 5.01 |
| **CaO** | 5.73 | 9.53 | 7.02 | 8.85 | 8.75 | 7.38 | 8.42 | 9.17 | 7.56 | 6.97 | 7.64 | 7.57 | 6.02 |
| **$Na_2O$** | 2.63 | 2.43 | 2.19 | 2.20 | 2.51 | 2.59 | 2.54 | 2.45 | 2.42 | 2.42 | 2.01 | 2.19 | 2.55 |
| **$K_2O$** | 2.43 | 0.36 | 0.74 | 0.58 | 1.07 | 1.01 | 1.39 | 0.71 | 0.59 | 0.54 | 0.22 | 1.13 | 1.19 |
| **MgO** | 2.73 | 2.91 | 2.34 | 4.49 | 2.86 | 2.31 | 2.97 | 3.04 | 2.52 | 2.66 | 3.83 | 2.07 | 2.32 |
| **$TiO_2$** | 0.62 | 0.66 | 0.65 | 0.87 | 0.86 | 0.62 | 0.71 | 0.86 | 0.50 | 0.57 | 0.69 | 0.67 | 0.63 |
| **MnO** | 0.11 | 0.11 | 0.16 | 0.13 | 0.13 | 0.11 | 0.11 | 0.13 | 0.16 | 0.15 | 0.12 | 0.04 | 0.11 |
| **$P_2O_5$** | 0.19 | 0.14 | 0.16 | 0.15 | 0.18 | 0.14 | 0.19 | 0.21 | 0.40 | 0.08 | 0.15 | 0.17 | 0.14 |
| **LOI** | 2.42 | 1.82 | 1.38 | 1.07 | 3.15 | 2.34 | 2.51 | 2.37 | 0.77 | 1.40 | 3.53 | 2.10 | 3.25 |
| | **Trace and rare earth elements (ppm)** | | | | | | | | | | | | |
| **Zr** | 130.96 | 105.21 | 135.19 | 129.79 | 151.86 | 107.05 | 145.39 | 143.18 | 104.06 | 128.92 | 240.00 | 159.92 | 159.09 |
| **La** | 9.89 | 3.26 | 2.29 | 5.14 | 8.14 | 4.47 | 6.31 | 6.66 | 5.87 | 2.96 | 4.47 | 6.15 | 3.1 |
| **Ce** | 15.63 | 3.17 | 1.54 | 5.88 | 11.52 | 5.09 | 6.75 | 6.85 | 5.58 | 1.5 | 4.41 | 7.82 | 3.01 |
| **Pr** | 2.16 | < 1 | < 1 | 1.14 | 1.81 | 1.05 | 1.24 | 1.36 | 1.29 | < 1 | 1.23 | 1.4 | < 1 |
| **Nd** | 8.2 | 3.1 | 2.65 | 4.49 | 7.17 | 3.89 | 4.37 | 4.73 | 4.87 | 2.26 | 3.61 | 4.77 | 3.06 |
| **Sm** | 1.36 | < 1 | < 1 | < 1 | 1.36 | < 1 | < 1 | < 1 | < 1 | < 1 | 4.69 | 1 | < 1 |
| **Eu** | 0.22 | < 0.1 | < 0.1 | < 0.1 | 0.25 | 0.13 | 0.12 | 0.15 | 0.18 | < 0.1 | 0.11 | 0.14 | < 0.1 |
| **Gd** | 1.29 | < 1 | < 1 | 1.06 | 1.3 | < 1 | < 1 | 1.09 | 1.31 | < 1 | 1.63 | 1.14 | < 1 |
| **Tb** | < 0.1 | < 0.1 | < 0.1 | < 0.1 | < 0.1 | < 0.1 | < 0.1 | < 0.1 | < 0.1 | < 0.1 | < 0.1 | < 0.1 | < 0.1 |
| **Dy** | 0.71 | 0.46 | 0.57 | 0.75 | 0.86 | 0.58 | 0.49 | 0.68 | 1.01 | 0.41 | 0.68 | 0.76 | 0.48 |
| **Ho** | < 0.1 | < 0.1 | < 0.1 | < 0.1 | < 0.1 | < 0.1 | < 0.1 | < 0.1 | 0.12 | < 0.1 | < 0.1 | < 0.1 | < 0.1 |
| **Er** | 0.32 | 0.19 | 0.27 | 0.4 | 0.43 | 0.24 | 0.22 | 0.33 | 0.62 | 0.18 | 0.29 | 0.42 | 0.21 |
| **Tm** | < 1 | < 1 | < 1 | < 1 | < 1 | < 1 | < 1 | < 1 | < 1 | < 1 | < 1 | < 1 | < 1 |
| **Yb** | < 1 | < 1 | < 1 | < 1 | < 1 | < 1 | < 1 | < 1 | < 1 | < 1 | < 1 | < 1 | < 1 |
| **Lu** | < 0.1 | < 0.1 | < 0.1 | < 0.1 | < 0.1 | < 0.1 | < 0.1 | < 0.1 | < 0.1 | < 0.1 | < 0.1 | < 0.1 | < 0.1 |
| **ΣREE** | 39.78 | 10.18 | 7.32 | 18.86 | 32.84 | 15.45 | 19.50 | 21.85 | 20.85 | 7.31 | 21.12 | 23.6 | 9.86 |

Al concentration is below 1% (0.58–1.84%) in some spots (Table 3), the average Ti the Al contents are more than 2% and 1%, respectively, indicating magmatic magnetite. The high Co concentration of more than 100 ppm in magnetite indicates a hydrothermal-magmatic source. The Co content in placer magnetites (130–161 ppm) suggests a hydrothermal-magmatic origin for them. Hydrothermal magnetites have low V concentrations (less than 1000 ppm) (Rusk et al. 2009). The V content in magnetites from volcanic rock fragments ranges from 0.38 to 1.51% (Table 3), which is similar to the V values of magmatic magnetite. In the placer magnetites from the Mahura deposit, however, the V content is less than 1000 ppm (93–208 ppm; Table 2), which may be due to the imprecision of the analysis of this element using the ICP-MS method. The low Cr concentration and high Ni/Cr ratio indicate hydrothermal magnetite (Dare et al. 2014). The Cr concentration in placer magnetites is between 204 and 281 ppm, and in magnetites from volcanic rock fragments it is between 0.01 and 0.09%. The Ni/Cr ratio in placer magnetites is between 0.17 and 0.22, while in magnetites from volcanic rock fragments it is 0 to 15.

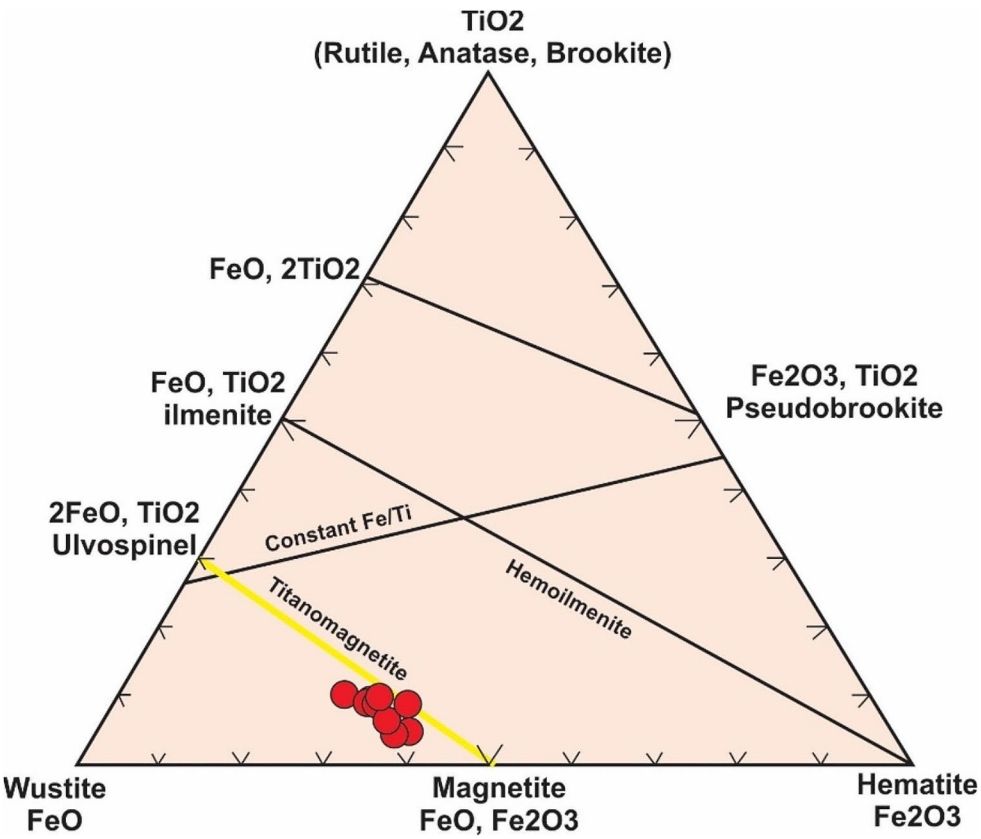


**Fig. 6** Composition of magnetites in the volcanic rock fragments from the Mahura area plotted in the $TiO_2$-$Fe_2O_3$-FeO system (Buddington and Lindsley 1964)

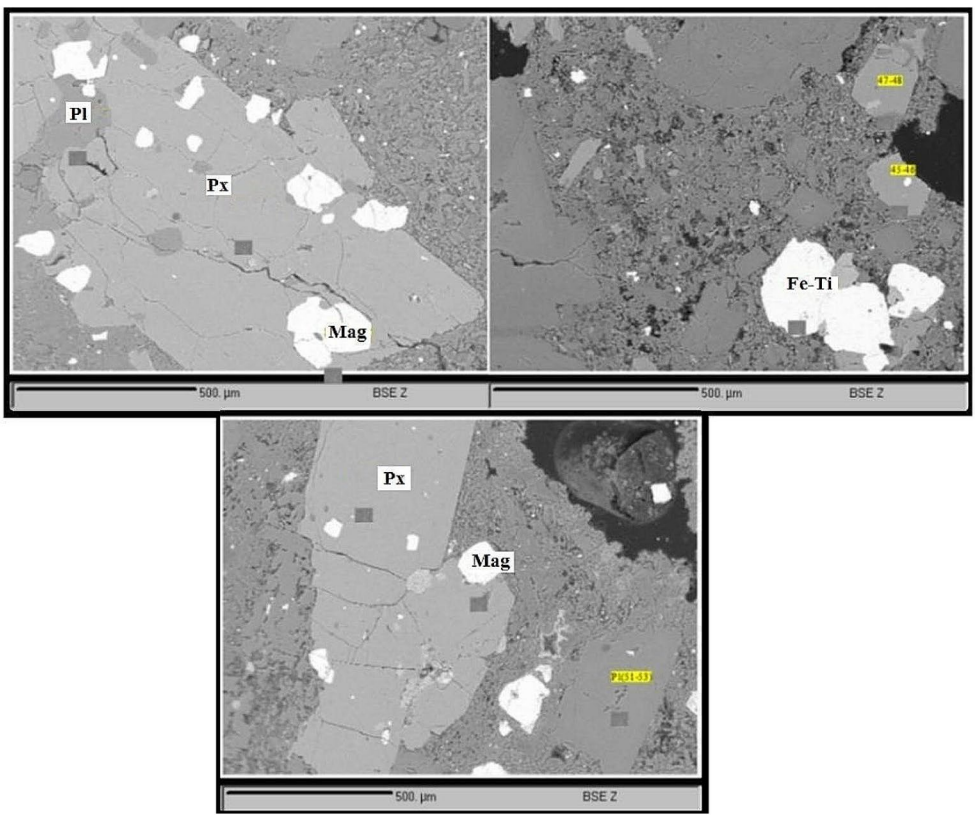


**Fig. 7** SEM-BSE images showing magnetite and titanomagnetite minerals in the volcanic rock fragments from the Mahura area. Px = pyroxene; Pl = plagioclase; Fe-Ti = titanomagnetite; and Mag = magnetite

The Cr content and the Ni/Cr ratio indicate that they do not depend on hydrothermal activities.

The Ti versus Al and Ti versus Ni/Cr ratio diagrams distinguish magmatic from hydrothermal magnetites, as magmatic magnetite has a high Ti and low Ni/Cr ratio compared to hydrothermal magnetite (Canil et al. 2016; Chen et al. 2019; Tao et al. 2022; Dare et al. 2014). Both placer magnetite and magnetite in volcanic rock fragments are plotted in the magmatic magnetite field (Fig. 8a and b), confirming a magmatic origin of magnetite. The Ni/(Cr + Mn) versus Ti + V and Ca + Al + Mn versus Ti + V diagrams are used to distinguish between different types of iron ore deposits (Dupuis and Beaudoin 2011). All magnetites from the Mahura area fall into the Fe-Ti, V domain (Fig. 8c and d), suggesting the same origin. In the V versus Ti diagram, the placer magnetites and the magnetites in the volcanic rock fragments are plotted in the area corresponding to the titaniferous iron ores, again showing the same source (Fig. 9; Loberg and Horndahal, 1983).

Finally, the fact that the chemistry of placer magnetites and magnetites in volcanic rock fragments lie in the same ranges of the diagrams for determining the origin of magnetite, points to the same source. Regarding the provenance of the Mahura placer magnetites, it should therefore be concluded that these magnetites were released by weathering and erosion of volcanic rock fragments and concentrated over time in the alluvium containing them.

## Provenance area of the volcanic rock fragments

As mentioned above, the Mahura iron placer deposit is located in the northeastern part of the Meyghan playa basin, where the area is covered by Quaternary alluvial sediments. The slope of the sedimentary basin and the direction of the alluvial fans indicate that the alluvium originated from the

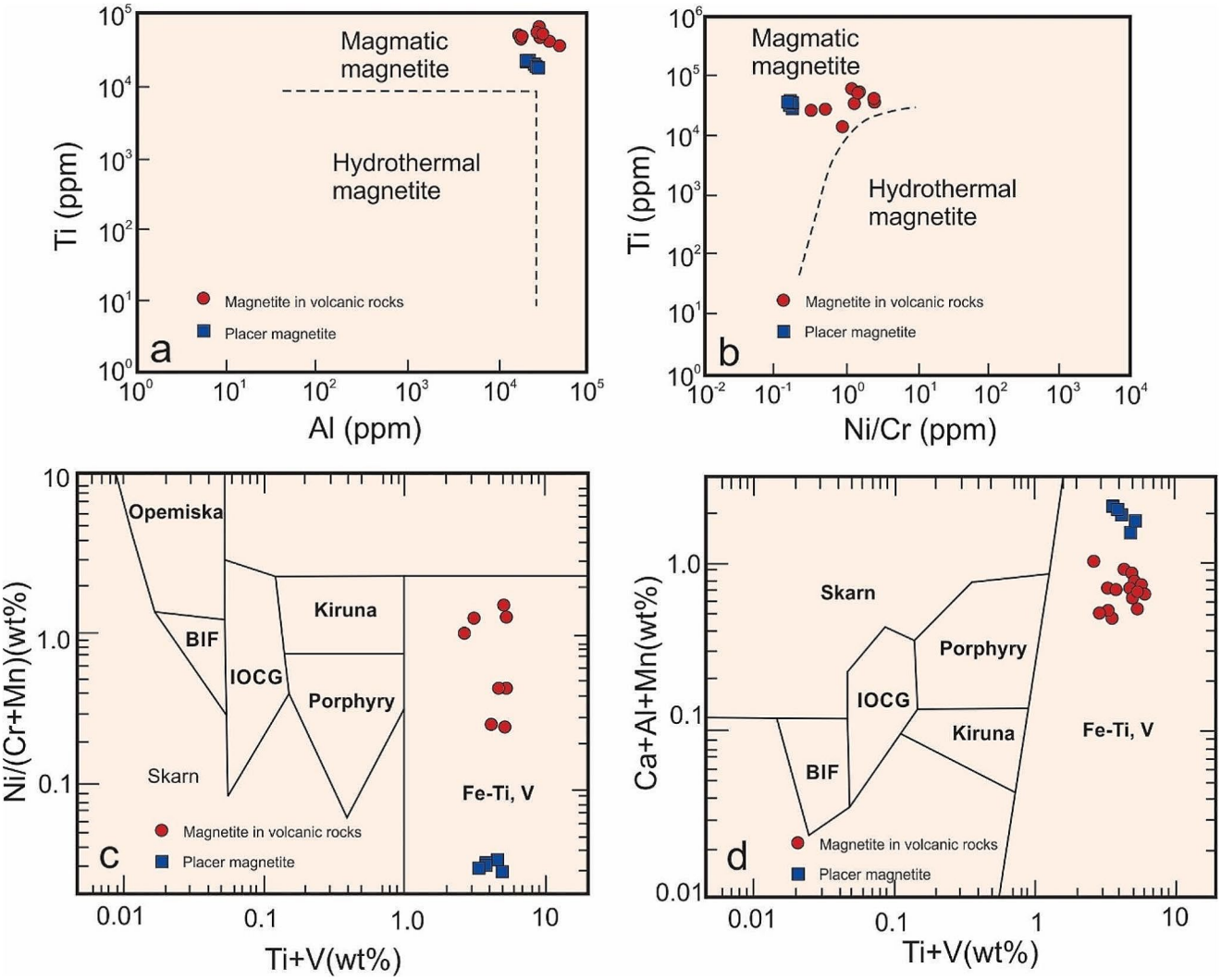


**Fig. 8** Ti versus Al (a; Canil et al. 2016), Ti versus Ni/Cr ratio (b; Dare et al. 2014), Ni/(Cr + Mn) versus Ti + V (c; Dupuis and Beaudoin 2011), and Ca + Al + Mn versus Ti + V (d; Dupuis and Beaudoin 2011) diagrams for the magnetite samples from the Mahura area

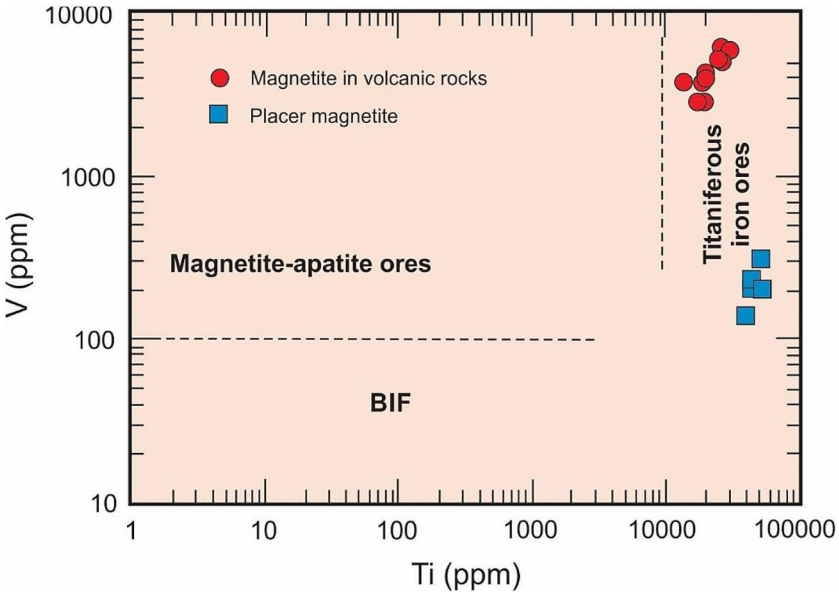


**Fig. 9** The V versus Ti diagram (Loberg and Horndahal, 1983) for the Mahura magnetite samples

northern area, i.e. the Ashtian Basin (Ghadimi and Esmaeli 2022). To investigate the possibility that the magnetite-bearing volcanic rock fragments originated from volcanic rocks that are widely distributed in the Ashtian region and throughout the Urumieh-Dokhtar Zone, the geochemistry of the volcanic rock fragments was compared with volcanic rocks from the Ashtian region (Zarei Sahamiyeh et al. 2008) in petrogenetic diagrams (Fig. 10). The volcanic rocks of Ashtian are found 30 km north of the Mahura area and consist of basaltic andesite, andesite, trachyandesite, dacite, rhyodacite and rhyolite (Zarei Sahamiyeh et al. 2008).

Based on the $SiO_2$ versus $Na_2O+K_2O$ diagram (Cox et al. 1979), the volcanic rock fragments fall within the andesite range, which is consistent with microscopic studies (Fig. 10a). Although the volcanic rocks of Ashtian comprise a broad spectrum of rock types, the Mahura's volcanic rock fragments overlap with the andesite part of this spectrum. In the $K_2O$-$SiO_2$ diagram (Peccerillo and Taylor 1976), most of the volcanic rock fragments are located in the tholeiitic and calc-alkaline series and overlap with the volcanics of the Ashtian Mountains (Fig. 10b). In the Ti-Zr diagram (Pearce and Cann 1973), both the studied samples and the Ashtian volcanic rocks lie in the area of the calc-alkaline basalts from the magmatic arcs (Fig. 10c). In addition, the chondrite-normalized REE patterns (Boynton 1984) of the volcanic rock fragments from the Mahura area and the Ashtian volcanic rocks are similar in terms of LREE enrichment and negative Eu anomaly (Fig. 10d). The same position of the Mahura volcanic rock fragments and the Ashtian volcanics in the petrogenetic diagrams and the similarity of the chondrite-normalized REE patterns for these rocks suggest that the magnetite-bearing volcanic rock fragments originate from the Ashtian area to the north of the Mahura iron placer deposit.

## Conclusions

In the Mahura iron placer deposit, magnetite occurs as micrometer-sized grains in the Quaternary alluvium, which consists of sandy, silty and clayey sediments as well as volcanic rock fragments. According to petrographic investigations and the whole-rock geochemistry, the volcanic rock fragments are predominantly andesite and basaltic andesite. The volcanic rock fragments contain magnetite as disseminated grains in their matrix and as inclusions in phenocrysts. The high Ti content suggests that the placer magnetites and magnetites in the volcanic rock fragments are dominantly titanomagnetite. The chemistry of the placer magnetites and the magnetites in the volcanic rock fragments in the discriminating elemental diagrams for different types of iron ore deposits indicates that both magnetites have the same origin. This finding suggests that erosion of the volcanic rock fragments over time has led to the release of the magnetite grains and their concentration as placer magnetites. The petrogenetic elemental diagrams show that the volcanic rock fragments in the alluvium and the volcanic rocks from the Ashtian Basin north of the Mahura deposit are similar in nature. This identity of the volcanic rocks indicates that the magnetite-bearing volcanic rock fragments originate from the Ashtian Mountains.

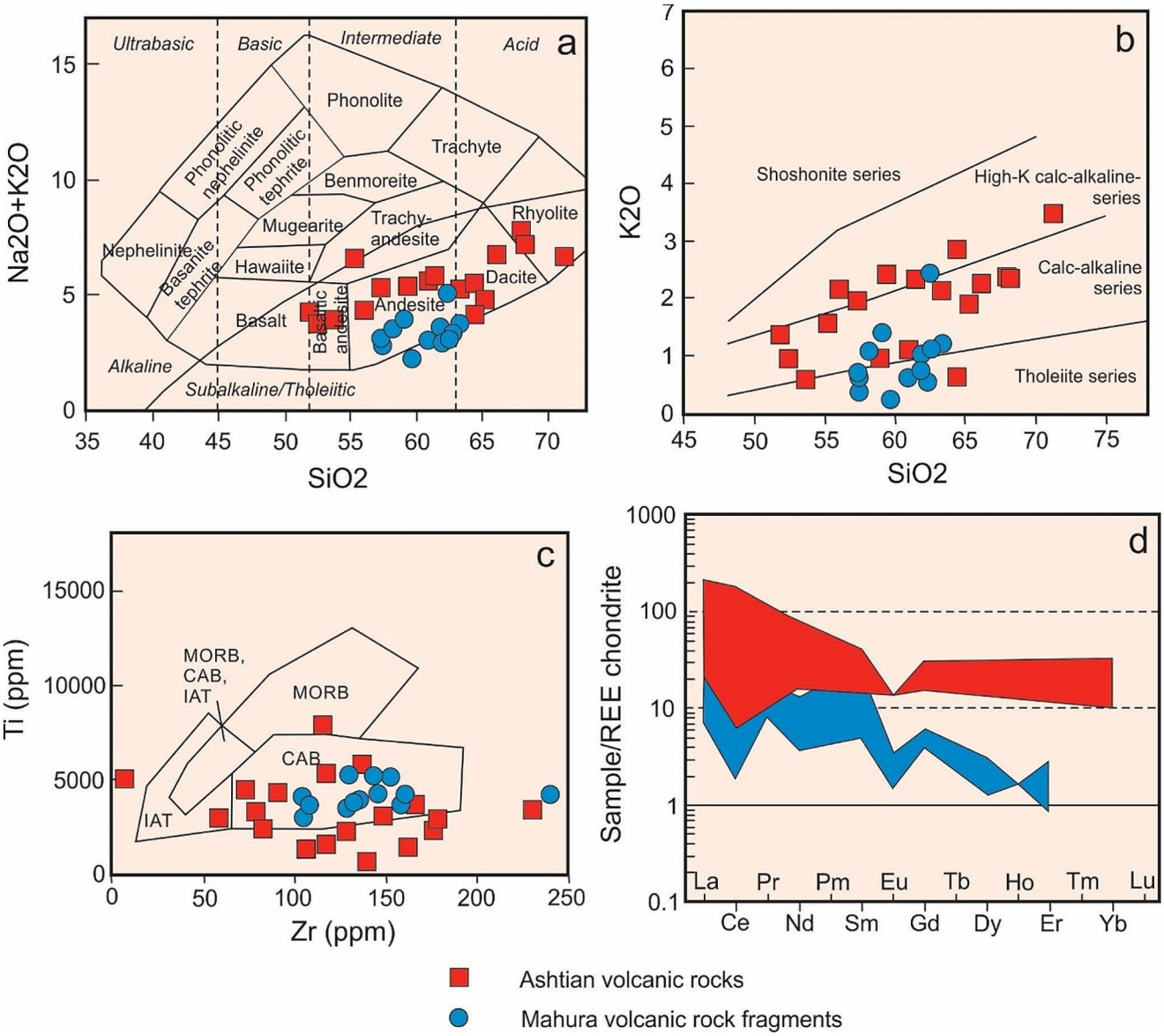


**Fig. 10** Petrogenetic diagrams for the volcanic rock fragments from the Mahura area and the Ashtian volcanics. (**a**) The $SiO_2$ versus $Na_2O+K_2O$ diagram (Cox et al. 1979); (**b**) The $K_2O$-$SiO_2$ diagram (Peccerillo and Taylor 1976); (**c**) The Ti-Zr diagram (Pearce and Cann 1973); and (**d**) The chondrite-normalized REE patterns (Boynton 1984). The data for Ashtian volcanics from Zarei Sahamiyeh et al. (2008)

**Acknowledgements** This study was conducted as a partial fulfilment of the requirements for a PhD in Economic Geology for the first author from Mahallat Branch, Islamic Azad University. We are grateful for the comments of two anonymous reviewers who improved the quality of the manuscript.

**Author contributions** Elham Firouzi: investigation, resources, writing—original draft preparation. Farhad Ehya: Conceptualization, investigation, data curation, writing—review and editing, supervision. Mohammad Ali Aliabadi: Conceptualization, data curation, writing—review and editing. Razieh Mohammadi: Conceptualization, data curation, writing—review and editing.

**Data availability** Data is provided within the manuscript.

## Declarations

**Ethical statement** The conducted research is not related to either human or animals use.

**Competing interests** The authors declare no competing interests.

## References

Alai Mahabadi S (2000) Salafchegan-Khorheh quadrangle map 1:100,000 series, sheet no. 6058. Geological Survey of Iran

Badkoubeh Hazaveh A, Rezaei K (2021) Enhancing of Quaternary iron-placer deposits by combining band ratio data of remote

sensing and magnetometry and geology by WOI method and comparison with SAM and FCC methods in the Hamedan 1:100,000 sheet. Quaternery J Iran 7:783–798 (in Persian)
Bedard E, Bronac D, de Vazelhes V, Beaudoin B (2022) Performance of predictive supervised classification models of trace elements in magnetite for mineral exploration. J Geochem Explor 236:106959
Bell AS, Simon A (2011) Experimental evidence for the alteration of the $Fe^{3+}/\Sigma Fe$ of silicate melt caused by the degassing of chlorine-bearing aqueous volatiles. Geology 39:499–502
Bookstrom AA (1995) Magmatic features of iron ores of the Kiruna type in Chile and Sweden; ore textures and magnetite geochemistry; discussion. Econ Geol 90:469–473
Boutroy E, Dare SAS, Beaudoin G, Barnes SJ, Lightfoot PC (2014) Magnetite composition in Ni-Cu-PGE deposits worldwide and its application tomineral exploration. J Geochem Explor 145:64–81
Boynton WV (1984) Geochemistry of the rare earth elements: meteorite studies. In: Henderson P (ed) Rare earth element geochemistry. Elsevier, pp 63–114
Buddington AF, Lindsley DH (1964) Iron-titanium oxide minerals and synthetic equivalents. J Petrol 5:310–357
Canil D, Grondahl C, Lacourse T, Pisiak LK (2016) Trace elements in magnetite from porphyry Cu–Mo–Au deposits in British Columbia, Canada. Ore Geol Rev 72:1116–1128
Carew MJ, Mark G, Oliver NHS, Pearson N (2006) Trace element geochemistry of magnetite and pyrite in Fe oxide (±Cu-Au) mineralized systems: insights into the geochemistry of ore-forming fluids: Geochimica et Cosmochimica Acta, v. 70, p. A83
Chen WT, Zhou MF, Li X, Gao JF, Hou K (2015) In-situ LA-ICP-MS trace elemental analyses of magnetite: Cu-(Au, Fe) deposits in the Khetri copper belt in Rajasthan Province, NW India. Ore Geol Rev 65:929–939
Chen W, Ying YC, Bai T (2019) Situ Major and Trace Element Analysis of Magnetite from Carbonatite-Related complexes: implications for Petrogenesis and Ore Genesis. Ore Geol Rev 107:30–40
Cox KG, Bell JD, Pankhurst RJ (1979) The interpretation of igneous rocks, 450p edn. London, Allen and Unwin
Cygan GL, Candela PA (1995) Preliminary study of gold partitioning among pyrrhotite, pyrite, magnetite, and chalcopyrite at 600 to 700°C, 140 MPa (1400 bars). In: Thompson JFH (ed) Magmas, fluids and Ore deposits, vol 23. Mineralogical Association of Canada Short Course, pp 129–137
Dare SAS, Barnes SJ, Beaudoin G (2012) Variation in trace element content of magnetite crystallized from a fractionating sulfide liquid, Sudbury, Canada: implications for provenance discrimination. Geochim Cosmochim Acta 88:27–50
Dare SAS, Barnes SJ, Beaudoin G, Méric J, Boutroy E, Potvin-Doucet C (2014) Trace elements in magnetite as petrogenetic indicators. Mineral Deposita 49:785–796
Dare SAS, Barnes SJ, Beaudoin G (2015) Did the massive magnetite lava flows of El Laco (Chile) form by magmatic or hydrothermal processes? New constraints from magnetite composition by LA-ICP-MS. Mineral Deposita 50:607–617
Dilles JH, Kent AJ, Wooden JL, Tosdal RM, Koleszar A, Lee RG, Farmer LP (2015) Zircon compositional evidence for sulfur-degassing from ore-forming arc magmas. Econ Geol 110:241–251
Dupuis C, Beaudoin G (2011) Discriminant diagrams for iron oxide trace element fingerprinting of mineral deposit types: Mineralium Deposita. 46:319–335
Ebrahimi M, Esmaeili R, Javad M, Farzadian H (2016) Placer iron mineralization in Zarnan area, east of Zanjan. The 8th conference of the Economic Geology Association of Iran, 7 pp. (in Persian with English abstract)
Ehsani Nasab P, Ehya F (2019) Mineralogy and magnetite trace element geochemistry of the Niyasar iron ore deposit, Esfahan Province, Iran. Periodico Di Mineralogia 88:59–73
Ghadimi F, Esmaeli F (2022) Textural and origin of Cheshmeh Khorzan conglomerate (Arak Meyghan Playa watershed) by multivariate statistical method. J Stratigraphy Sedimentology Researches 38:99–114 (in Persian with extended English abstract)
Ghasemi A, Talbot CJ (2006) A new tectonic scenario for the Sanandaj-Sirjan Zone, Iran. J Asian Earth Sci 26:683–693
Groves DI, Bierlein FP, Meinert LD, Hitzman MW (2010) Iron oxide copper-gold (IOCG) deposits through Earth history: implications for origin, lithospheric setting, and distinction from other epigenetic iron oxide deposits. Econ Geol 105:641–654
Hajalilou B, Razmara M, Hajalilou N (2021) Identification of the origin of Ataieh vanadium-bearing titanomagnetite minerals in southwest Mashhad by XRM, SEM and EPMA methods. Geosciences 31:53–64 (in Persian with English abstract)
Haldar SK (2013) Chap. 2 - economic Mineral deposits and host rocks, editor(s): S.K. Haldar, Mineral Exploration. Elsevier, pp 23–39
Heidarian H, Alirezaei S, Lentz DR (2017) Chadormalu Kiruna-type magnetite-apatite deposit, Bafq district, Iran: insights into hydrothermal alteration and petrogenesis from geochemical, fluid inclusion, and sulfur isotope data. Ore Geol Rev 83:43–62
Hosseinzadeh M, Alizadeh M, Hosseini MR (2017) Mineralogical and physical beneficiation studies for iron extraction from Bardaskan Titanomagnetite Placer deposit. J Min Environ 8:191–201
Hu H, Li JW, Lentz D, Ren Z, Zhao XF, Deng XD, Hall D (2014) Dissolution–reprecipitation process of magnetite from the Chengchao iron deposit: insights into ore genesis and implication for in-situ chemical analysis of magnetite. Ore Geol Rev 57:393–405
Hu X, Chen H, Zhao L, Han J, Xia X (2017) Magnetite geochemistry of the Longqiao and Tieshan Fe–(Cu) deposits in the Middle-Lower Yangtze River Belt: implications for deposit type and ore genesis. Ore Geol Rev 89:822–835
IMIMT (Iranian Ministry of Industry Mining and Trade), 2012. Exploitation license of Mahura placer magnetite deposit. (in Persian)
Jahantigh M, Shahraki N (2014) Estimation and evaluation of iron deposits placer, Bazman, South-East of Iran. The 6th conference of the Economic Geology Association of Iran, 9 pp. (in Persian with English abstract)
Karimpour M (1989) Applied Economic Geology. Javid Publication, Mashhad, Iran, p 404. (in Persian)
Lindsley DH (1991) Experimental studies of oxide minerals. Rev Mineral 25:69–106
Loberg BE, Horndahl AK (1983) Ferride geochemistry of Swedish precambrian iron ores. Miner Deposita 18:487–504
Marbouti Z, Ehya F, Rostami Paydar G, Maleki S (2020) Geochemical, microthermometric, and sulfur isotopic constraints on the origin of the Sarviyan iron deposit, Markazi Province, Iran. J Geochem Explor 210:106451
Mitwally EMA, Yu BS (2022) Geochemistry of magnetite in beach sands, stream sediments, and in situ magnetites in surrounding rocks at north Taiwan island. Acta Geochim 41:434–452
Moinevaziri H, Mirza TA (2021) Characteristics and origin of iron mineralization in Northern Sanandaj -Sirjan Zone (Iran -Iraq). Iraqi Bull Geol Min 17:43–58
Morison SR (1989) Placer deposits in Canada. In: Fulton RJ (ed) Quaternary geology of Canada and Greenland. Geology of Canada, Geological Survey of Canada, Ottawa, pp 687–694
Nabatian G, Rastad E, Neubauer F, Honarmand M, Ghaderi M (2015) Iron and Fe–Mn mineralisation in Iran: implications for Tethyan metallogeny. Aust J Earth Sci 62:211–241
Nadoll P, Mauk JL, Hayes TS, Koenig AE, Box SE (2012) Geochemistry of magnetite from hydrothermal ore deposits and host rocks of the Mesoproterozoic Belt Supergroup, United States. Econ Geol 107:1275–1292
Nadoll P, Angerer T, Mauk JL, French D, Walshe J (2014) The chemistry of hydrothermal magnetite: a review. Ore Geol Rev 61:1–32

Nadoll P, Mauk JL, Leveille RA, Koenig AE (2015) Geochemistry of magnetite from porphyry Cu and Skarn deposits in the southwestern United States. Mineral Deposita 50:493–515

Nourani F, Razmara M, Hajalilou B (2011) The Provenance of VTM ore deposit of Sangerd area (SW Neyshabour) by EPMA and SEM. The 30th National Geosciences Congress, 8 pp. (in Persian with English abstract)

Pearce JA, Cann JR (1973) Tectonic setting of basic volcanic rocks determined using trace element analyses. Earth Planet Sci Lett 19:290–300

Peccerillo A, Taylor SR (1976) Geochemistry of Eocene calc-alkaline volcanic rocks from the Kastamonu area, northern Turkey. Contrib Miner Petrol 58:63–81

Ray GE, Webster ICL (2007) Geology and chemistry of the low Ti magnetite-bearing heff Cu-Au skarn and its associated plutonic rocks, Heffley Lake, south-central British Columbia. Explor Min Geol 16:159–186

Rusk BG, Oliver N, Brown A, Lilly R, Jungmann D (2009) Barren magnetite breccias in the Cloncurry region, Australia; comparisons to IOCG deposits: Society for Geology Applied to Mineral Deposits, 10th Biennial SGA Meeting, Townsville, Australia, 2009, Proceedings, pp. 656–658

Samari H, Tavakoli A, Jalali M, Asadi A (2014) Petrological, petrographical and geochemical studies to determine the genesis of iron ore, placer deposit, Arak city. The 8th National Specialized Geology Conference of Payam Noor University, 9 pp., (in Persian with English abstract)

Sievwright RH, Wilkinson JJ, O'Neill HSC, Berry AJ (2017) Thermodynamic controls on element partitioning between titanomagnetite and andesitic–dacitic silicate melts. Contrib Miner Petrol 172:1–33

Simon AC, Candela PA, Piccoli PM, Mengason M, Englander L (2008) The effect of crystal-melt partitioning on the budgets of Cu, au, and Ag. Am Mineral 93:1437–1448

Singoyi B, Danyushevsky L, Davidson G, Large R, Zaw K (2006) Determination of trace elements inmagnetites from hydrothermal deposits using the LA–ICP-MS technique. SEG Keystone Conference, Denver, USA CD-ROM

Sossi PA, Prytulak J, O'Neill HSC (2018) Experimental calibration of vanadium partitioning and stable isotope fractionation between hydrous granitic melt and magnetite at 800° C and 0.5 GPa. Contrib Miner Petrol 173:27

Sutherland DG (ed) (1991) Alluvial mining. Institution of Mining and Metallurgy, Elsevier Applied Science, London, p 601

Tao L, Zhang H, Wu J, Zhou X, Zhang L (2022) Magma Generation of Magnetite-Rich Intermediate-Mafic rocks and its Mantle processes in the Southwestern Alxa Block, NW China. J Earth Sci 33(1):161–176

Toplis MJ, Carroll MR (1995) An experimental study of the influence of oxygen fugacity on Fe-Ti oxide stability, phase relations, and mineral—melt equilibria in ferro-basaltic systems. J Petrol 36:1137–1170

Toplis MJ, Corgne A (2002) An experimental study of element partitioning between magnetite, clinopyroxene and iron-bearing silicate liquids with particular emphasis on vanadium. Contrib Miner Petrol 144:22–37

Ward LA, Holwell DA, Barry TL, Blanks DE, Graham SD (2018) The use of magnetite as a geochemical indicator in the exploration for magmatic Ni-Cu-PGE sulfide deposits: a case study from Munali. Zambia J Geochem Explor 188:172–184

Wechsler BA, Lindsley DH, Prewitt CT (1984) Crystal structure and cation distribution in titanomagnetites ($Fe_3$-x$TixO_4$). Am Mineral 69:754–770

Xiaoxu Z, Juxing T, Bin L, Qin W, Liang H, Gang Y, Rui S, Qiang W, Qiu D, Pingcuo Z (2023) Geochemistry of magnetite from the Mamupu Cu polymetallic deposit, Yulong belt, Tibet: implications for magnetite genesis, stages and mechanism of formation. Ore Geol Rev 154:105334

Yi J, Shi X, Ji G, Zhang L, Wang S, Deng H (2024) The Geochemical Characteristics of Trace Elements in the Magnetite and Fe Isotope Geochemistry of the Makeng Iron Deposit in Southwest Fujian and their significance in Ore Genesis. Minerals 14:217

Zarei Sahamiyeh R, Tabasi H, Jalali M (2008) Investigation of petrology and tectonomagmatic environment of Ashtian volcanic rocks. Tarbiat Moalem Univ Sci J 8:227–240 (in Persian)

Zhang D, Rusk B, Oliver N, Dai T (2011) Trace element geochemistry of magnetite from the Ernest Henry IOCG deposit, Australia. 11th biennial meeting SGA 2011-Let s talk ore deposits, Antofagasta, Chile